J. Fluid Mech. (2025), *vol.* 1014, A23, doi:10.1017/jfm.2025.10228

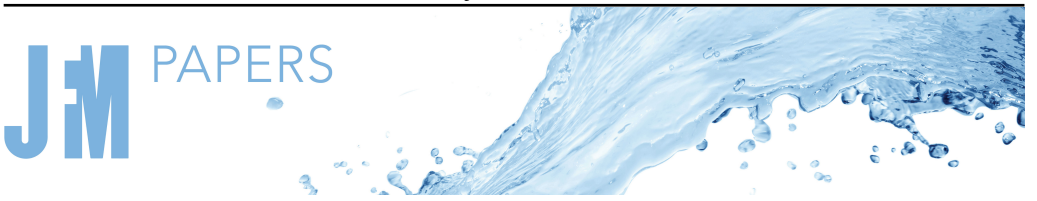

Modulation leading to frequency downshifting of water waves in the vicinity of the Benjamin–Feir transition

Daniel James Ratliff[1], **Olga Trichtchenko**[2] **and Thomas J. Bridges**[3]

[1]Department of Mathematics, Physics and Electrical Engineering, Northumbria University, Newcastle upon Tyne NE1 8ST, UK

[2]Department of Physics and Astronomy, The University of Western Ontario, London, Ontario, N6G 2V4, Canada

[3]School of Mathematics and Physics, University of Surrey, Guildford GU2 7XH, UK

Corresponding author: Daniel James Ratliff, daniel.ratliff@northumbria.ac.uk

(Received 22 October 2024; revised 4 March 2025; accepted 3 May 2025)

For Stokes waves in finite depth within the neighbourhood of the Benjamin–Feir stability transition, there are two families of periodic waves, one modulationally unstable and the other stable. In this paper we show that these two families can be joined by a heteroclinic connection, which manifests in the fluid as a travelling front. By shifting the analysis to the setting of Whitham modulation theory, this front is in wavenumber and frequency space. An implication of this jump is that a permanent frequency downshift of the Stokes wave can occur in the absence of viscous effects. This argument, which is built on a sequence of asymptotic expansions of the phase dynamics, is confirmed via energetic arguments, with additional corroboration obtained by numerical simulations of a reduced model based on the Benney–Roskes equation.

Key words: surface gravity waves, hamiltonian theory, variational methods

1. Introduction

One of the most celebrated instabilities in fluid dynamics is the Benjamin–Feir instability, where a Stokes wavetrain, travelling uniformly in finite depth, undergoes a transition from stability to instability as the depth of the fluid increases. The original papers (Benjamin 1967; Benjamin & Feir 1967) have attracted significant attention in the years since their first publication. Nevertheless it continues to fascinate, and there is still much to learn about its implications. One such phenomenon, known now as frequency downshifting,

emerged in experiments following up on the Benjamin–Feir result. These experimental investigations of monochromatic wavetrains (e.g. Lake *et al.* 1977; Melville 1982; Su *et al.* 1982; Huang, Long & Shen 1996) demonstrated that energy is exchanged from the primary wave mode to other sideband frequencies. As this process begins to arrest, these experiments observed that the dominant peak of the wave power occurred not at the original carrier-wave frequency, but one of a lower frequency, namely that the frequency peak had moved down the spectrum to lower frequencies (and thus the nomenclature). In this paper we focus on modulation and dynamics of water waves near the Benjamin–Feir transition, and find that the frequency downshifting phenomenon emerges naturally via phase dynamics.

The conventional explanation as to how this phenomenon emerges is via dissipative effects, such as wind forcing or inherent viscous effects, and these explanations have been supported by numerical simulations (Lo & Mei 1985; Hara & Mei 1991; Dias & Kharif 1999; Carter & Govan 2016; Carter, Henderson & Butterfield 2019). It was thought that permanent frequency downshifting was not possible in purely conservative systems (Lo & Mei 1985; Hara & Mei 1991; Dias & Kharif 1999). However, as with all nonlinear paradigms, more than one mechanism can lead to the same phenomenon. There is a growing consensus that frequency downshifting can indeed be observed without energy dissipation or forcing (Onorato *et al.* 2002; Dysthe *et al.* 2003; Janssen 2003; Chalikov 2007, 2012; Shugan *et al.* 2019). Whilst some of these alternative mechanisms have been observed numerically, an open question remains as to the theoretical explanation for downshifting to occur without dissipation.

In this paper we propose a new mechanism for frequency downshifting for inviscid and irrotational water waves without dissipation. The theory is based on asymptotically valid modulation equations, building on classical Whitham modulation theory and its generalisations. Whitham modulation theory has a distinct advantage over nonlinear Schrödinger equation models (e.g. Hasimoto & Ono 1972; Johnson 1977; Kakutani & Michihiro 1983) in that it is precisely the wavenumber and frequency that are modulated, thereby generating equations that inherently contain jumps in frequency. In the conservative setting, it is singularities that provide the mechanism for downshifting. The primary singularity is coalescence of two characteristics in the Whitham modulation equations at the Benjamin–Feir transition (Whitham 1967).

One has to go beyond Whitham (1967) as higher-order modulation equations are required in order to capture the nonlinear implications of the double characteristic, which is what we achieve here within this paper. Our strategy is to re-scale and re-modulate to obtain new asymptotically valid modulation equations near the Benjamin–Feir threshold. In Bridges & Ratliff (2017, 2021) a general theory for the re-modulation of Whitham theory in the neighbourhood of coalescing characteristics is constructed. There it is found that the conservation of wave action in Whitham theory is instead replaced by a two-way Boussinesq equation for the modulation wavenumber, with the modulation frequency coming in via the equation for conservation of waves. However, this theory needs modification as a secondary singularity arises at the Benjamin–Feir transition, changing the nonlinearity in the two-way Boussinesq equation from quadratic to cubic. The resulting modulation equation, first derived in Ratliff (2017), is

$$\alpha_1 U_{TT} + \alpha_2 (U^3)_{XX} + \alpha_3 (2UU_T + U_X \partial_X^{-1} U_T)_X + \alpha_4 U_{XXXX} = 0\,, \tag{1.1}$$

where U characterises the local wavenumber, T, X are slow time and space scales and $\alpha_1, \ldots, \alpha_4$ are real-valued parameters. It is the key equation in this paper, as it is asymptotically valid and contains travelling fronts which connect two wavenumber states

thereby capturing the frequency downshifting via conservation of waves. The properties and analysis of (1.1) are given in § 4.

There are several steps in the analysis leading from the generic Whitham theory to (1.1). The first step is to introduce a general form for the secondary modulation of the Stokes wave and mean flow. The form of the phase, wavenumber and frequency modulation is cast in vector form as

$$\begin{pmatrix}\theta\\ \phi_0\end{pmatrix}=\begin{pmatrix}k_0x-\omega_0t\\ u_0x-\gamma_0t\end{pmatrix}+\varepsilon^{\alpha}\boldsymbol{\Theta}(X,T)\,,$$

$$\begin{pmatrix}k\\ u\end{pmatrix}=\begin{pmatrix}k_0\\ u_0\end{pmatrix}+\varepsilon^{\alpha+1}\boldsymbol{K}(X,T)\,,\qquad \begin{pmatrix}\omega\\ \gamma\end{pmatrix}=\begin{pmatrix}\omega_0\\ \gamma_0\end{pmatrix}+\varepsilon^{\alpha+1}c\mathbf{K}+\varepsilon^{\alpha+\beta}\boldsymbol{\Omega}(X,T)\,, \tag{1.2}$$

$$\text{with}\quad X=\varepsilon(x-ct),\quad T=\varepsilon^{\beta}t\quad\text{and}\quad \varepsilon\ll 1\,,$$

where k_0, ω_0 are the wavenumber and frequency of the Stokes wave and u_0, γ_0 are the bulk velocity and Bernoulli constant of the mean flow. The speed c is a characteristic speed obtained from the generic Whitham modulation equations using the standard approach (Whitham 2011). The quantity θ is the phase of the wave, and ϕ_0 is referred to as the pseudo-phase of the mean flow, due to its resemblance to a wave phase and playing a similar role in the Whitham modulation equation. The exponents α and β are determined by ensuring that the equations are asymptotically valid, and that the modulation wavenumber and frequencies are in balance:

$$\boldsymbol{\Theta}_X=\boldsymbol{K}\quad\text{and}\quad\boldsymbol{\Theta}_T=-\boldsymbol{\Omega}\,. \tag{1.3}$$

We will look at two cases of the re-modulation. The first is with scales $\alpha=1$ and $\beta=3$. These values are relevant in the hyperbolic region, where all four characteristics in Whitham (1967) are real, and

$$c=c_g\pm\sqrt{\omega_0''(k_0)\omega_2^{eff}(k_0)a}+\dots\,, \tag{1.4}$$

with $\omega_0''\omega_2^{eff}>0$, where a denotes the wave amplitude and ω_2^{eff} is the (Stokes) frequency correction to the Stokes wave, including mean flow. In this region we find that re-modulation leads to Korteweg de-Vries (KdV) dynamics, with the modulation equation taking the universal form (Ratliff 2021)

$$\Delta'(c)\left[U_T+\kappa UU_X+\frac{1}{6}\sigma'''(0)U_{XXX}\right]=0\,, \tag{1.5}$$

with U characterising the evolution of the vector-valued wavenumber via $\boldsymbol{K}=\zeta U(X,T)$ and ζ is the right eigenvector of the Whitham modulation equations. Thus, the re-modulation slaves the slow evolution of the wave and mean flow to one another within the water-wave problem. The new modulation dynamics is characterised by properties of the wavetrain via the characteristic polynomial of the Whitham modulation equations $\Delta(c)$ and the Bloch spectrum of the wave $\sigma(\nu)$ (Doelman *et al.* 2009). The coefficient of the quadratic nonlinearity is

$$\kappa=\begin{pmatrix}\mathrm{D}_{\mathbf{k}}c(\mathbf{k},\boldsymbol{\omega})\\ \mathrm{D}_{\boldsymbol{\omega}}c(\mathbf{k},\boldsymbol{\omega})\end{pmatrix}\cdot\begin{pmatrix}\boldsymbol{\zeta}\\ c\boldsymbol{\zeta}\end{pmatrix}\,, \tag{1.6}$$

where $c(\mathbf{k},\boldsymbol{\omega})$ is a modulation (characteristic) speed and D denotes a directional (Gateaux) derivative, which can be interpreted as the linearised version of Lax's genuine nonlinearity criterion for the Whitham modulation equations (Ratliff 2021). The analysis leading to this equation, as well as the definitions of $\Delta(c)$ and Bloch spectrum $\sigma(\nu)$, are given in § 3.

It is important to note that the KdV equation (1.5) is not the famous KdV equation in shallow-water hydrodynamics (Korteweg & De Vries 1895)! It is a KdV equation describing perturbations of the Stokes wave and the mean flow, and not just long-wave perturbations to the free surface and velocity (i.e. just the mean flow in the absence of a background wave). This KdV equation is of interest here because in the limit to the Benjamin–Feir transition, the coefficient κ of the quadratic nonlinearity goes to zero, signalling the change from quadratic to cubic nonlinearity. This KdV equation may also have independent interest in giving an alternative explanation for the appearance of dark solitary waves in shallow-water hydrodynamics (cf. Bridges & Donaldson 2006).

In summary, the argument for frequency downshifting takes three steps. Firstly, generic Whitham modulation theory gives the characteristics with two of these changing type from hyperbolic to elliptic at the Benjamin–Feir transition. Secondly, re-modulation in the hyperbolic region generates KdV dynamics on top of the Stokes wave and mean flow. Taking the limit to the Benjamin–Feir transition then leads to a third modulation equation (1.1) for the wavenumber, and its jump solutions generate frequency downshifting (or, in principle, upshifting). Whilst this paper will focus on the water-wave problem as the key application of the above abstract theory, the theory is more general as it applies to a basic periodic wavetrain of any amplitude, as long as it has at least two phases. The secondary modulation then is applicable. This form of frequency downshifting is universal in that the theory is formulated independent of any particular equation, as long as it is conservative and generated by a Lagrangian. However, in this paper the focus is on the Benjamin–Feir transition.

An outline of the paper is as follows. In § 2 the theory for re-modulation is set up and those aspects of Whitham (1967) that feed into the higher-order modulation equations are highlighted. Then in § 3 the KdV equation on a Stokes wave (1.5) is derived and analysed. It is valid everywhere in the hyperbolic region of generic Whitham theory, and we are interested in its behaviour near the hyperbolic–elliptic transition which signals the onset of Benjamin–Feir instability. In § 3 we also introduce the concept of Bloch spectrum which arises in the derivation of the dispersive term both in (1.5) and in (1.1). In § 4 the key properties of (1.1) are highlighted, and the analysis leading to jumps in wavenumber and frequency is given. Further support for the new theory of frequency downshifting is presented in § 5 using energy arguments, and in § 6 by direct simulation of the Benney–Roskes equation. We find that the downshifted wavetrain is the state with the lower energy, providing an energetic argument for why downshifting is observed and persistent even in conservative systems. In the concluding remarks section we summarise the main result, and indicate some generalisations.

2. Stokes waves, modulation and characteristics

In this section, we set up the basic state and its properties. The basic state is a Stokes wave on finite depth coupled to mean flow. The starting point for the analysis is the inviscid, irrotational model for gravity waves in finite depth h_0 and constant density. The governing equations for the velocity potential $\phi(x, y, t)$ and the free surface deflection $\eta(x, t)$ on the domain $(x, y, t) \in \mathbb{R} \times [-h_0, \eta] \times [0, \infty)$ are

$$\phi_{xx} + \phi_{yy} = 0\,, \quad \text{for } y \in (-h_0, \eta)\,, \tag{2.1a}$$

$$\phi_y(x, -h_0, t) = 0\,, \tag{2.1b}$$

$$\eta_t + \phi_x \eta_x = \phi_y\,, \quad \text{at } y = \eta\,, \tag{2.1c}$$

$$\phi_t + \frac{1}{2}|\nabla\phi|^2 + g\eta = 0\,, \quad \text{at } y = \eta\,, \tag{2.1d}$$

where g is the acceleration due to gravity. These equations are conservative and can be obtained from the first variation of a Lagrangian:

$$\delta L = 0\,, \quad \text{with} \quad L = \int\int \left(\int_{-h_0}^{\eta} \phi_t + \frac{1}{2}|\nabla\phi|^2 + gy \,\mathrm{d}y \right) \mathrm{d}x\,\mathrm{d}t. \tag{2.2}$$

The evaluation of $\delta L = 0$ is given in § 13.2 of Whitham (2011). Now consider a Stokes expansion for the velocity potential and free surface:

$$\begin{aligned} \eta(\theta) &= b + a\cos(\theta) + \sum_{n=2}^{\infty} a_n \cos(n\theta)\,, \\ \phi(y,\theta) &= \Phi + \sum_{n=1}^{\infty} \frac{A_n}{n} \cosh(nk(y+h_0))\sin(n\theta), \end{aligned} \tag{2.3}$$

with phases θ and Φ given by

$$\theta = kx - \omega t \quad \text{and} \quad \Phi = ux - \gamma t\,. \tag{2.4}$$

The constants $k,\ \omega$ (representing the wavenumber and frequency) and $u,\ \gamma$ (representing the horizontal fluid velocity and Bernoulli head) parametrise the wave and the mean flow, respectively. The parameters a and b parametrise the amplitudes of the surface Stokes wave and mean fluid deflection from rest (i.e. $\eta = 0$), respectively.

The quantity θ is the usual phase of the wavetrain, whereas Φ is called a pseudo-phase, although mathematically it is equivalent to the wave phase (cf. § 3.1 in Bridges & Ratliff (2021)). The pseudo-phase arises from an affine symmetry in ϕ present in the Lagrangian. The above solution, therefore, can be treated as a relative equilibrium with two phases – one associated with the translation invariance in phase of the Lagrangian, and the other due to the affine symmetry of the velocity potential. The presence of these mean flow effects facilitates the inclusion of the bulk mode b in the expansion of η, which alters the mean (i.e. period-averaged) fluid depth to $h_0 + b$ in response to mean-flow effects primarily driven by u and γ. This therefore leads to two 'triads' in the modulation theory – (k, ω, a) characterising the surface Stokes wave and (u, γ, b) for the mean-flow effects. As we will see within this paper, the two triads couple, and it is this coupling that drives the dynamics which leads to downshifting in the vicinity of the Benjamin–Feir instability.

Substitution of the above wave–mean-flow solution into the Lagrangian, averaging over one period of the wave and solving the resulting system of equations for the Fourier coefficients a_n and A_n, one is able to obtain the following averaged Lagrangian, to leading order in E and b:

$$\mathscr{L} = \left(\frac{u^2}{2} - \gamma \right)(h_0 + b) + \frac{1}{2} g b^2 + D(k, u, \omega)E + \mu E\, b + \frac{1}{2}\tau E^2 + \mathcal{O}\big(b^2,\, E^3,\, E^2 b\big)\,. \tag{2.5}$$

The two small parameters are the energy density $E = (1/2)ga^2$ and mean deflection b from the quiescent position $\eta = 0$. This reduced Lagrangian is derived in Whitham (1967) and has been confirmed in Bridges & Ratliff (2022).

The function D is the right-moving linear dispersion relation with a mean flow component

$$D(k, u, \omega) = \frac{1}{2}\left(1 - \frac{(\omega - uk)^2}{\omega_0^2} \right), \quad \text{where} \quad \omega_0^2 = gk\tanh(kh_0). \tag{2.6}$$

It has a root at $\omega = uk + \omega_0(k)$. The constants μ and τ in (2.5) are

$$\mu = \frac{B_0}{c_0 h_0} \quad \text{and} \quad \tau = \frac{k^2}{g}\left(\frac{9T_0^4 - 10T_0^2 + 9}{8T_0^4}\right), \tag{2.7}$$

with

$$B_0 = c_g - \frac{c_0}{2}, \quad c_g = u + \omega_0'(k), \quad c_0 = \frac{\omega_0}{k} \quad \text{and} \quad T_0 = \tanh(kh_0). \tag{2.8}$$

Primes represent derivatives with respect to the wavenumber k. Variations of the Lagrangian (2.5) with respect to E and b, when set to zero, yield the weakly nonlinear dispersion relations

$$D + \mu b + \tau E = 0, \qquad \gamma = \frac{u^2}{2} + gb + \mu E. \tag{2.9}$$

In the absence of mean variations (i.e. $b = 0$), the first can be solved to find the conventional low-amplitude Stokes expansion of the frequency:

$$\omega = uk + \omega_0(k) + \omega_2^0 E + \mathcal{O}(E^2), \tag{2.10}$$

where the Stokes frequency correction in the absence of bulk/mean-flow variations, ω_2^0, is given by

$$\omega_2^0 = \omega_0 \tau = \frac{k^2 \omega_0}{g}\left(\frac{9T_0^4 - 10T_0^2 + 9}{8T_0^4}\right) = \frac{k^3}{\omega_0}\left(\frac{9T_0^4 - 10T_0^2 + 9}{8T_0^3}\right) = \frac{k^2}{c_0}\Lambda, \tag{2.11}$$

where the expression Λ is precisely D_0 in Whitham (1967), but the notation has been altered to prevent confusion. The dependence of ω_2^0 on k is important and will be retained here as derivatives of ω_2^0 with respect to these parameters appear in the analysis, at leading order. Therefore, it is convenient to establish $\tau = \omega_0^{-1}\omega_2^0$, and thus we may write the coupled system (2.9) as

$$\begin{pmatrix} \mu & \tau \\ g & \mu \end{pmatrix}\begin{pmatrix} b \\ E \end{pmatrix} = \begin{pmatrix} -D \\ \gamma - \frac{u^2}{2} \end{pmatrix}. \tag{2.12}$$

Henceforth, all expressions and coefficients within the paper, unless explicitly stated otherwise, will be evaluated at $\omega = uk + \omega_0(k)$. It is assumed henceforth that these equations are non-degenerate:

$$\Delta_W = \mu^2 - g\tau = \frac{B_0^2}{c_0^2 h_0^2} - \frac{g\omega_2^0}{\omega_0} \neq 0. \tag{2.13}$$

Indeed, this expression is negative-definite for gravity waves (but may change sign in other water-wave problems, such as when surface tension or variable density is present). This equation clearly demonstrates that the energy density E and bulk variation b are truly independent, and not constrained as previously suggested in § 16.9 of Whitham (2011). The independence of b and E play an important role in the phase modulation of the Stokes waves, when E and b are slowly varying functions. The precise leading-order effect of the mean velocity field on the wave component is given in Appendix A. Further, this system prescribes E and b as functions of the wave and mean-flow parameters k, ω, u and γ, which are required for the phase dynamical reduction.

2.1. *Modulating wave and mean flow*

In classical Whitham modulation theory (Whitham 1967), applied to the wave mean-flow problem, the key parameters

$$\boldsymbol{\Theta} = \begin{pmatrix} \theta \\ \Phi \end{pmatrix}, \quad \mathbf{k} = \begin{pmatrix} k \\ u \end{pmatrix}, \quad \boldsymbol{\omega} = \begin{pmatrix} \omega \\ \gamma \end{pmatrix} \tag{2.14}$$

are allowed to be slowly varying functions:

$$\begin{gathered} \boldsymbol{\theta} \to \boldsymbol{\theta} + \varepsilon^{-1}\boldsymbol{\Theta}(X,T), \quad \mathbf{k} \to \mathbf{k} + \boldsymbol{K}(X,T), \quad \boldsymbol{\omega} \to \boldsymbol{\omega} + \boldsymbol{\Omega}(X,T), \\ \text{where} \quad X = \varepsilon(x - ct), \quad T = \varepsilon t \quad \text{and} \quad \varepsilon \ll 1. \end{gathered} \tag{2.15}$$

The coupled Whitham modulation equations are then

$$\mathbf{K}_T = \boldsymbol{\Omega}_X \quad \text{and} \quad \frac{\partial}{\partial T}\mathbf{A}(\boldsymbol{\omega} + \boldsymbol{\Omega}, \mathbf{k} + \mathbf{K}) + \frac{\partial}{\partial X}\mathbf{B}(\boldsymbol{\omega} + \boldsymbol{\Omega}, \mathbf{k} + \mathbf{K}) = 0 \tag{2.16}$$

(cf. equation (1.14) of Bridges & Ratliff (2021)), where the first equation is the so-called 'conservation of waves' and the second is the conservation of wave action for each phase. As such, $\mathbf{A}$ and $\mathbf{B}$ are denoted as the vector-valued wave action and wave action flux, respectively:

$$\mathbf{A} = -\mathrm{D}_{\boldsymbol{\omega}}\mathscr{L} \quad \text{and} \quad \mathbf{B} = \mathrm{D}_{\mathbf{k}}\mathscr{L}. \tag{2.17}$$

Differentiating $\mathscr{L}$ in (2.5) and substituting into (2.17) gives the components of the wave action conservation law:

$$\begin{gathered} \mathbf{A} = -\mathrm{D}_{\boldsymbol{\omega}}\mathscr{L} = \begin{pmatrix} -D_\omega E \\ h_0 + b \end{pmatrix}, \quad \mathbf{B} = \mathrm{D}_{\mathbf{k}} \quad \mathscr{L} = \begin{pmatrix} D_k E + \mu' E b + \frac{1}{2}\tau' E^2 \\ u(h_0 + b) + D_u E \end{pmatrix}, \\ \text{where} \quad (\mathrm{D}_{\boldsymbol{x}} F)\boldsymbol{y} = \lim_{s \to 0}\left(\frac{F(\boldsymbol{x} + s\boldsymbol{y}) - F(\boldsymbol{x})}{s}\right). \end{gathered} \tag{2.18}$$

To compute characteristics, we will need the linearisation of (2.16). Differentiating (2.16) with respect to $\boldsymbol{\Omega}$ and $\mathbf{K}$, linearising and introducing the characteristic form

$$\boldsymbol{\Omega}(X,T) = \widehat{\boldsymbol{\Omega}}\mathrm{e}^{\mathrm{i}(X+cT)} \quad \text{and} \quad \mathbf{K}(X,T) = \widehat{\mathbf{K}}\mathrm{e}^{\mathrm{i}(X+cT)} \tag{2.19}$$

results in an eigenvalue problem for the characteristics c:

$$\left[\begin{pmatrix} -\mathrm{D}_{\boldsymbol{\omega}}\mathbf{A} & \mathbf{0} \\ \mathbf{0} & \mathrm{D}_{\mathbf{k}}\mathbf{B} \end{pmatrix} + c\begin{pmatrix} \mathbf{0} & \mathrm{D}_{\boldsymbol{\omega}}\mathbf{A} \\ D_{\boldsymbol{\omega}}\mathbf{A} & \mathrm{D}_{\mathbf{k}}\mathbf{A} + \mathrm{D}_{\boldsymbol{\omega}}\mathbf{B} \end{pmatrix}\right]\begin{pmatrix} \widehat{\boldsymbol{\Omega}} \\ \widehat{\mathbf{K}} \end{pmatrix} = \begin{pmatrix} \mathbf{0} \\ \mathbf{0} \end{pmatrix}. \tag{2.20}$$

This equation is an example of the general form of the equation for characteristics in multiphase Whitham modulation theory (cf. equation (1.18) in Bridges & Ratliff (2021)). It is assumed in this construction that $D_{\boldsymbol{\omega}}\mathbf{A}$ is invertible, and the first equation in (2.20) has been multiplied by this matrix.

Combining the two equations in (2.20) by eliminating $\widehat{\boldsymbol{\Omega}}$, and defining $\boldsymbol{\zeta} = \widehat{\mathbf{K}}$, reduces this equation to the matrix pencil:

$$\mathbf{E}(c)\boldsymbol{\zeta} = 0, \quad \boldsymbol{\zeta} = \begin{pmatrix} \zeta_1 \\ \zeta_2 \end{pmatrix}. \tag{2.21}$$

The roots of $\det(\mathbf{E}(c)) = 0$ are the characteristics of the modulation equations for the Stokes wave mean-flow interaction. The general form of the 2×2 matrix $E(c)$ is

$$\mathbf{E}(c) = \mathrm{D}_{\mathbf{k}}\mathbf{B} + c(\mathrm{D}_{\boldsymbol{\omega}}\mathbf{B} - \mathrm{D}_{\mathbf{k}}\mathbf{A}) - c^2\mathrm{D}_{\boldsymbol{\omega}}\mathbf{A} := \begin{pmatrix} E_{11} & E_{12} \\ E_{12} & E_{22} \end{pmatrix}, \tag{2.22}$$

and explicit expressions for the entries E_{11}, E_{12} and E_{22} for the water-wave problem are given in Appendix B.

From this pencil, we find the characteristic polynomial for the Stokes wave mean-flow modulation is

$$\begin{aligned}
\Delta(c) &= \det(\mathbf{E}(c)) \\
&= (c-c_g)^2\big(gh_0 - (u-c)^2\big) - 2\omega_0(c-c_g)\big(gh_0 - (c-u)^2\big)\mu' b \\
&\quad - E\left\{\omega_0''\Omega + 2(c-c_g)\left[\omega_0(gh_0-(c-u)^2)\tau' - \frac{B_0+(c-u)}{\omega_0}\mu'\right.\right. \\
&\quad \left.\left. -\frac{\omega_0'}{\omega_0}\Omega + \frac{(gh_0 + B_0(c-u))}{c_0h_0}\left(\frac{\omega_0'}{c_0} - 1\right)\right]\right\} \\
&\quad + \mathcal{O}\big(E^2, Eb, b^2, (c-c_g)^2E, (c-c_g)^2b\big),
\end{aligned} \tag{2.23}$$

where

$$\Omega(c;k,u) = \omega_2^0\big(gh_0 - (c-u)^2\big) - \frac{k}{c_0h_0}\big(B_0^2 + 2B_0(c-u) + gh_0\big). \tag{2.24}$$

This polynomial has four roots, admitting four characteristics, and we will find explicit expressions for them in the small amplitude limit $E \ll 1$. Two of these characteristics are associated with the group velocity of the wave, whereas the final two are related to the linear long-wave speeds. It is the former that we are interested in, as these are the ones which correspond to the Benjamin–Feir instability. The two characteristics of (2.23) that are associated with the group velocity, for small amplitude, are found to be

$$c = u + \omega_0' \pm \sqrt{\omega_0''\omega_2^{eff}E} + C_2E + \omega_0\mu' b + \mathcal{O}\big(E^{3/2}, Eb, b^2\big), \tag{2.25}$$

where

$$\omega_2^{eff} = \frac{\Omega(c_g;k,u)}{gh_0 - \omega_0'^2} = \frac{k}{c_0h_0}\left[kh_0\Lambda - \left(\frac{B_0^2 + 2B_0\omega_0' + gh_0}{gh_0 - \omega_0'^2}\right)\right], \tag{2.26}$$

and we have defined for brevity

$$C_2 = \big(\omega_2^0\big)' + \frac{B_0\omega_0' + gh_0}{c_0h_0\big(gh_0 - \omega_0'^2\big)}\left(\frac{k\big(B_0+\omega_0'\big)}{gh_0 - \omega_0'^2}\omega_0'' - 1\right) - \frac{\big(B_0+\omega_0'\big)}{gh_0 - \omega_0'^2}\frac{(kB_0)'}{c_0h_0}. \tag{2.27}$$

This expression for ω_2^{eff} is what is called $\Omega_2(k)$ in § 16.11 in Whitham (2011). However, the way it has emerged in this analysis is surprising, as the assumptions are different. In Whitham's analysis, one must either identify several terms in the analysis and modulation equations to neglect on consistency or size arguments (as in Whitham (1967)) or appeal to the flux induced by the waves via an argument proposed by Longuet-Higgins in order to arrive at the correct frequency expression (as done in Whitham (2011)), which essentially

constrains the mean induced by the waves b to be related to the energy density E. The relative equilibrium approach here, which maintains the independence of b and E, does not require this additional information and suggests that the result in Whitham is in fact a consequence of the symmetries of the Lagrangian and thus inherent to the problem itself.

We also need the eigenvector of $\mathbf{E}(c)$ when c is a characteristic, in the asymptotic limit $E \to 0$. In the neighbourhood of the double characteristic, the unfolding of the critical point is of $\mathcal{O}(E^{1/2})$. In the equation $\mathbf{E}(c)\boldsymbol{\zeta} = 0$ the characteristic (2.25) is substituted in for c and $\boldsymbol{\zeta}$ is expanded in powers of $E^{1/2}$. The details of this expansion can be found in (B2) of Appendix B. Evaluating this eigenvector at the Benjamin–Feir transition $kh_0 1.363$, it becomes

$$\boldsymbol{\zeta} = \sqrt{E}\left[C_2\boldsymbol{\chi} - \begin{pmatrix} \frac{\omega_0'}{c_0} - 1 + \frac{1}{\Delta_W}\left(\omega_2^0\omega_0' + \frac{kB_0}{c_0h_0}\right)\mu' - \frac{k\left(B_0\omega_0' + gh_0\right)}{h_0\Delta_W}\tau' \\ \omega_0'' \end{pmatrix}\right] + \mathcal{O}\left(E^{3/2}\right), \tag{2.28}$$

with

$$\boldsymbol{\chi} = -\frac{1}{c_0h_0\Delta_W}\begin{pmatrix} gh_0 + B_0\omega_0' \\ 0 \end{pmatrix}. \tag{2.29}$$

This eigenvector evaluated at the transition value simplifies to

$$\boldsymbol{\zeta} = \begin{pmatrix} 0.9252 \\ 2.1703h_0^{3/2} \end{pmatrix} a + \mathcal{O}(a^3), \tag{2.30}$$

since $E = (1/2)ga^2$.

2.2. *Bloch spectrum*

As can be see from (1.1) and (1.5), a key component of the phase dynamical construction associated with the coefficient of dispersion in the problem is the Bloch spectrum $\sigma(\nu)$, with ν the spatial Floquet exponent/Bloch wavenumber, for the Stokes wave solution. The Bloch spectrum consists of the eigenvalues of the linearisation of the full water-wave problem about the Stokes wave and has a central place in understanding the stability of Stokes waves in finite depth (Deconinck & Oliveras 2011; Berti *et al.* 2023; Creedon & Deconinck 2023; Berti *et al.* 2024), and so it is unsurprising that it features as a component of the phase dynamics reduction. In this paper only third-order dispersive effects are required in the asymptotic analysis because only the third-order Taylor coefficient of the Bloch spectrum about the zero Bloch wavenumber is required. In this section we identify an appropriate choice for the Bloch spectrum that is both analytically tractable and representative of the problem.

Due to the low-amplitude nature of the Stokes waves within this paper, it would be fair to expect the spectrum that arises from such problems to be akin to the spectrum of nonlinear Schrödinger-type models:

$$\sigma_{HNLS}(\nu) = c_g\nu + \frac{\omega_0'''}{6}\nu^3 \pm \nu\sqrt{\omega_0''\omega_2^{eff}E + \frac{1}{4}\omega_0''^2\nu^2}\,, \tag{2.31}$$

where the subscript $HNLS$ indicates that this is the exact spectrum for the nonlinear Schrödinger equation with higher-order dispersion terms (Ratliff 2021). To leading order in E and without higher-order dispersive effects, this expansion has been shown the same in the full water-wave problem in the vicinity of the Benjamin–Feir instability (Bridges &

Mielke 1995). However, the mean-flow effects in nonlinear Schrödinger models are treated adiabatically and as such may not be captured fully in this Bloch spectrum. To remedy this we compare this nonlinear Schrödinger Bloch spectrum with a model where the mean flow is non-adiabatic, which within this paper is the one obtained from the Benney–Roskes equation, given by (Benney & Roskes 1969)

$$iA_T + \epsilon\left(A_{XX} - \omega_2|A|^2A - kWA - \frac{gk^2-\omega_0^4}{2g\omega_0}BA\right) = 0, \tag{2.32}$$

$$B_T - c_gB_X + h_0W_X + \frac{gk^2-\omega_0^4}{\omega_0^2}(|A|)_X^2 = 0, \tag{2.33}$$

$$W_T - c_gW_X + gB_X + \frac{2gk}{\omega_0}\left(|A|^2\right)_X = 0\,. \tag{2.34}$$

In this equation, A is the complex amplitude of the wave, B is the mean level variation and W is the mean velocity. The small parameter ϵ (which differs from ε in the modulation theory) gives the order of magnitude of the wave amplitude. It is equivalent to the smallness of the parameter a and thus allows one to relate the Bloch spectrum of the Benney–Roskes system to the modulation theory of this paper. Whilst the full closed-form expression for the spectrum is complicated, we only require its long-wave expansion, which in terms of the Stokes wave parameters reads

$$\sigma_{BR}(\nu) = c\nu \pm \left(\frac{\omega_0''^2}{8\sqrt{\omega_0''\omega_2^{eff}E}} + \Xi\right)\nu^3 + \mathcal{O}(\nu^5), \tag{2.35}$$

where the characteristic c is defined as in (2.25) and

$$\Xi = \frac{g\omega_0''^3k\left(\left(3c_g^2+gh_0\right)\left(B_0^2+2B_0c_g+gh_0\right)+4B_0c_g\left(gh_0-c_g^2\right)\right)}{4c_0h_0\left(gh_0-c_g^2\right)^2\sqrt{\omega_0''\omega_2^{eff}}}\sqrt{E} + \mathcal{O}(E) \tag{2.36}$$

characterises the additional dispersive effects due to the mean flow. We note that this spectrum only differs from the long-wave expansion of the classical nonlinear Schrödinger equation at $\mathcal{O}(\sqrt{E})$, but does not alter the Benjamin–Feir instability boundary. As such, we postulate that we may augment the above spectrum with the third-order dispersive term in (2.31). (Formally, this can be done by following asymptotic procedures such as in Slunyaev (2005) or Kakutani & Michihiro (1983), noting that the mean-flow effects on the stability have already been accounted for.) This gives the Bloch spectrum that we utilise within this paper:

$$\sigma(\nu) = c\nu + \left(\pm\frac{\omega_0''^2}{8\sqrt{\omega_0''\omega_2^{eff}E}} \pm \Xi + \frac{\omega_0'''}{6}\right)\nu^3 + \mathcal{O}(\nu^5). \tag{2.37}$$

3. Phase modulation in the hyperbolic region

The hyperbolic region is the region in which Stokes waves coupled to mean flow exist and the Whitham modulation equations, linearised about the Stokes wave (2.20), have four real characteristics. Everywhere in this region the modulation can be re-scaled as in

(1.2) to derive the KdV equation (1.5). This KdV equation is in a characteristic moving frame with the speed determined by a characteristic from the generic Whitham theory. The theory for this re-modulation follows Ratliff & Bridges (2016*a*) and Ratliff (2019, 2021). The form for the re-modulation is (1.2) with $\alpha = 1$ and $\beta = 3$. The velocity potential and free surface are expressed as

$$Z(x,\, y,\, t) = \widehat{Z}\big(\boldsymbol{\theta} + \varepsilon\boldsymbol{\Theta}(X,\, T);\, \mathbf{k} + \varepsilon^2\mathbf{K}(X,\, T),\, \boldsymbol{\omega} + \varepsilon^2 c\mathbf{K} + \varepsilon^3\boldsymbol{\Omega}\big) + \varepsilon^4 W(X,\, T,\, \varepsilon), \tag{3.1}$$

where $Z(x,\, y,\, t) = (\phi(x,\, y,\, t),\, \eta(x,\, t))$, $\widehat{Z}(\boldsymbol{\theta};\, \mathbf{k},\, \boldsymbol{\omega})$ is the Stokes wave plus mean flow and c is one of the wave characteristics in the hyperbolic region:

$$c = c_g \pm \sqrt{\omega_0''(k_0)\omega_2^{eff}(k_0)}a + \cdots \quad \text{with} \quad \omega_0''(k_0)\omega_2^{eff}(k_0) > 0\,. \tag{3.2}$$

The modulation equations are then obtained by substitution of the above Stokes wave solution with these perturbed wave quantities into the water-wave equations and solving the resulting system at each order of the small parameter ε. The strategy is given in Ratliff & Bridges (2016*a*) and Ratliff (2019) and so we skip details. The resulting KdV equation has the form given in (1.5), which we repeat here as we evaluate the key coefficients:

$$\Delta'(c)\left[U_T + \kappa U U_X + \frac{1}{6}\sigma'''(0)U_{XXX}\right] = 0\,. \tag{3.3}$$

The function $U(X,\, T)$ in (3.3) is obtained by projection of $\mathbf{K}(X,\, T)$ in the direction of the eigenvector $\boldsymbol{\zeta}$ of $\mathbf{E}(c)\boldsymbol{\zeta} = 0$ with $\mathbf{E}(c)$ defined in (2.21) with its argument evaluated at (3.2):

$$\mathbf{K}(X,\, T) = U(X,\, T)\boldsymbol{\zeta}\,. \tag{3.4}$$

It is important to note that this KdV equation is not the classical KdV equation in shallow water, which can also be derived using phase dynamics (Bridges 2014), but the coefficients and implications are different. This is because in addition to perturbing the mean-free-surface level and horizontal velocity that the classical KdV would suggest, it additionally alters the wavenumber, frequency and amplitude of the surface Stokes wavetrain with non-zero amplitude. Indeed, the solitary wave solution of (1.5) is in fact a dark solitary wave (bi-asymptotic to a Stokes travelling wave). Hence the hyperbolic region is not only filled with modulationally stable Stokes waves, it is also filled with dark solitary waves, each moving at its local characteristic speed (3.2).

The coefficient $\Delta(c)$ is defined in (2.23), and its derivative is found to be

$$\Delta'(c) = \pm 2\big(gh_0 - \omega_0'^2\big)\sqrt{\omega_0''\omega_2^{eff}E} + \mathcal{O}\big(E^{3/2}\big). \tag{3.5}$$

The second important term is the dispersive term $\sigma'''(0)$ in the KdV equation, which is obtained from the Bloch spectrum. The Bloch spectrum is the temporal eigenvalue $\sigma(\nu)$ of the linearisation of the full equations considered as a function of the spatial Floquet exponent (see also § 2.2). Using the spectrum (2.37), we can readily obtain

$$\frac{1}{6}\sigma'''(0) = \pm\frac{\omega_0''^2}{8\sqrt{\omega_0''\omega_2^{eff}E}} \pm \Xi + \frac{\omega_0'''}{6} + \mathcal{O}(E). \tag{3.6}$$

Note that although this expression appears to be singular at the Benjamin–Feir transition $\omega_0''\omega_2^{eff} = 0$ the singularity is of the same order as the zero of $\Delta'(c)$ at this point, meaning the dispersive term in the KdV equation is finite and non-zero at this transition.

The third coefficient of interest is the coefficient κ of the nonlinearity:

$$\kappa = \begin{pmatrix} \mathrm{D}_{\mathbf{k}} c(\mathbf{k}, \boldsymbol{\omega}) \\ \mathrm{D}_{\boldsymbol{\omega}} c(\mathbf{k}, \boldsymbol{\omega}) \end{pmatrix} \cdot \begin{pmatrix} \boldsymbol{\zeta} \\ c\boldsymbol{\zeta} \end{pmatrix} . \tag{3.7}$$

This latter expression is related to the concept of genuine nonlinearity of the Whitham modulation equations, in the sense of Lax (cf. Lax 1973; Ratliff 2021). Evaluation of this coefficient for the water-wave problem is straightforward but lengthy. Using the expressions (2.25) and (B2) we can show that

$$\begin{aligned} \kappa = \mp \frac{3}{2} \mathscr{M}_1 \sqrt{\omega_0'' \omega_2^{eff}} - \sqrt{E} \left\{ \omega_0'' \left[\frac{\omega_0'}{c_0} + \frac{\mathscr{M}_1}{2} \left(\left(\omega_2^{eff} \right)' + 4C_2 - 2\tau' \omega_0 \right) \right] \right. \\ \left. + \omega_2^{eff} \left[\frac{1}{2} \mathscr{M}_1 \omega_0''' + \omega_0'' \left(\frac{3(\omega_0' \mu)'}{2\Delta_W} + \frac{\omega_0'}{\omega_0} \mathscr{M}_1 - \frac{g(k\omega_0' - 3\omega_0)}{2\omega_0^2 \Delta_W} \right) \right] \right\} \\ + \mathcal{O}(E) . \end{aligned} \tag{3.8}$$

The coefficient $\mathscr{M}_1$ is given in equation (A2) of Appendix A where it is associated with the change of wave properties due to mean velocity changes. The coefficient of the nonlinearity κ is finite at the Benjamin–Feir transition, and so once multiplied by (3.5) the quadratic term in the KdV equation will vanish. This is important at the Benjamin–Feir transition, and is the reason that the nonlinearity within the phase dynamical description goes from purely quadratic as in (1.5) to involving the cubic and mixed quadratic terms seen in (1.1).

In summary, in the Benjamin–Feir stable region, the KdV equation which emerges, for the faster of the two characteristic speeds, is

$$\sqrt{\omega_0'' \omega_2^{eff}} E \left(U_T + \kappa U U_X \right) - \left[\frac{\omega_0''^2}{8} + \left(\Xi + \frac{\omega_0'''}{6} \right) \sqrt{\omega_0'' \omega_2^{eff}} E \right] U_{XXX} = 0. \tag{3.9}$$

This KdV equation is asymptotically correct to order E. However the KdV equation does not support heteroclinic connections, thereby precluding jumps in frequency and wavenumber. This is known for two reasons. The first is by considering solutions of permanent form. By utilising the Hamiltonian structure of the KdV equation, one finds the heteroclinic connection of permanent form must satisfy

$$\alpha U_\xi^2 + \beta U^3 - V U^2 + I U \equiv \alpha U_\xi^2 + \mathcal{V}(U) = 0 \tag{3.10}$$

for coefficients α, β, wave speed V, travelling coordinate $\xi = X - VT$ and integration constant I. Unlike heteroclinic connections (which require one simple and one repeated root), heteroclinic connections require two saddle notes to exist in the above dynamical system, equivalent to $\mathcal{V}$ possessing two double roots (Kamchatnov *et al.* 2012), which is impossible for a cubic polynomial. Any step-like solution that is not of permanent form is known to disintegrate into a train of solitary waves in the long-time limit (Hruslov 1976; Venakides 1986). Hence, in the strictly hyperbolic (modulationally stable) regime there cannot be a permanent change in wavenumber.

As noted above, it is apparent from the expressions for the coefficients that the first two terms of this KdV equation are zero whenever $\omega_2^{eff} = 0$, occurring exactly at the Benjamin–Feir transition, which signifies a change in scale. This inevitably leads to at least cubic nonlinearities emerging, although quadratic nonlinearities of mixed type (i.e. involving spatial and temporal derivatives) are *a priori* also anticipated. This theory is developed in

the next section, resulting in a modified version of the two-way Boussinesq equation. This new modulation equation will have the necessary nonlinearities and dispersion to support a heteroclinic connection that will lead to downshifting of the Stokes waves.

4. Phase modulation near the Benjamin–Feir transition

In approaching the Benjamin–Feir transition, two singularities arise. Firstly, two characteristics coalesce as noted in § 2 and secondly, the coefficient of the quadratic nonlinearity vanishes as noted in § 3. In light of this we utilise time scaling typically used to derive two-way Boussinesq equations, used to rebalance the time portion of the dynamics (Ratliff & Bridges 2016*b*), in tandem with scalings used to obtain the modified KdV equation where cubic terms resolve vanishing quadratic nonlinearities (Gear & Grimshaw 1983; Ratliff 2021). Therefore, in the re-modulation the coalescing characteristics change in light of the above observations, the first resulting in the small time exponent changing from $\beta = 3$ to $\beta = 2$ and the second a change of perturbation scales from $\alpha = 1$ to $\alpha = 0$. With the loss of quadratic nonlinearity and emergence of cubic nonlinearity new terms appear in the equation as shown in (1.1) rewritten here in a different form:

$$\alpha_1 U_{TT} + \left(\alpha_2 U^3 + \alpha_4 U_{XX}\right)_{XX} + \alpha_3 \left(2UU_T + U_X \partial_X^{-1} U_T\right)_X = 0\,. \tag{4.1}$$

The first three terms are the two-way Boussinesq equation with a cubic nonlinearity. The latter term, multiplied by α_3, is required to balance the cubic nonlinearity. With U of order ε, X of order ε and T of order ε^2, the three nonlinear terms are in balance:

$$\left(U^3\right)_{XX} \sim \varepsilon^5\,, \quad (UU_T)_X \sim \varepsilon^5 \quad \text{and} \quad \left(U_X \partial_X^{-1} U_T\right)_X \sim \varepsilon^5. \tag{4.2}$$

A detailed derivation of this equation is given in § 4.5.3 of Ratliff (2017) for the case of the laboratory frame, but can be extended to the case of the characteristic moving frame using recent works by the authors (most notably, Bridges & Ratliff 2017; Ratliff 2021). The dependent variable U is again obtained as a projection of the wavenumber onto the eigenvector, $\mathbf{K} = U\boldsymbol{\zeta}$, as in (3.4), although here the eigenvector is that associated with coalesced characteristics.

General expressions for the parameters in (4.1) are given in terms of the averaged Lagrangian in equation (4.27) of Ratliff (2017); however, the more accessible way to compute this number is to use the connection of the coefficients to the Bloch spectrum and expansions of the flux vector as in Ratliff (2021). The evaluations of the coefficients for the water-wave problem at the Benjamin–Feir transition are lengthy, and results are summarised here. The dispersion coefficient is

$$\alpha_4 = -\frac{\omega_0''^2}{4}\left(gh_0 - \omega_0'^2\right). \tag{4.3}$$

The time derivative term, which goes from a first-order derivative to a second-order derivative at the Benjamin–Feir transition, has coefficient

$$\alpha_1 = -\tfrac{1}{2}\Delta''(c) = \omega_0'^2 - gh_0\,. \tag{4.4}$$

The most complicated coefficient is that multiplying the cubic nonlinearity. Evaluating the formula on the weakly nonlinear Stokes wave gives

$$\alpha_2 = \frac{1}{2}\left[\Delta''\kappa^2 + \kappa\left[\begin{pmatrix} \mathrm{D}_{\mathbf{k}}\Delta' \\ \mathrm{D}_{\boldsymbol{\omega}}\Delta' \end{pmatrix} \cdot \begin{pmatrix} \boldsymbol{\zeta} \\ c\boldsymbol{\zeta} \end{pmatrix}\right]\right] = -\frac{\kappa\omega_0''}{12\Delta_W}\left(\left(\omega_2^{eff}\right)' + 4C_2\right)\Delta''\,. \tag{4.5}$$

At the Benjamin–Feir transition, κ reduces to

$$\kappa = -\sqrt{E}\omega_0'' \left[\frac{\omega_0'}{c_0} + \frac{\mathscr{M}_1}{2} \left(\left(\omega_2^{eff} \right)' + 4C_2 - 2\tau' \omega_0 \right) \right] + \mathcal{O}(E). \tag{4.6}$$

The last coefficient to compute is for the quadratic terms, which emerge due to the simultaneous vanishing of the time and nonlinear terms in the KdV term. This has the coefficient

$$\alpha_3 = \Delta'' \kappa. \tag{4.7}$$

Overall, this gives the modified two-way Boussinesq equation as

$$\begin{aligned} &U_{TT} + \beta_1 (U^3)_{XX} + \beta_2 \left(2UU_T + U_X \partial_X^{-1} U_T \right) + \beta_3 U_{XXXX} = 0\,, \\ \text{with} \quad &\beta_1 = \frac{\kappa \omega_0''}{6\Delta_W} \left[\left(\omega_2^{eff} \right)_k + 4C_2 \right] \sqrt{E}, \\ &\beta_2 = -2\kappa, \\ &\beta_3 = \frac{\omega_0''^2}{4}. \end{aligned} \tag{4.8}$$

The remaining depth and amplitude effects, to leading order, can be removed with the rescaling

$$T = \sqrt{\frac{h_0}{g}}\tau\,, \quad X = h_0 \chi\,, \quad U = \left(h_0 \sqrt{E} \right)^{-1} \mathcal{U}\,, \tag{4.9}$$

reducing the phase dynamical equation at the Benjamin–Feir transition point to simply

$$\mathcal{U}_{\tau\tau} - \left(0.1195 \mathcal{U}^3 - 0.02247\, \mathcal{U}_{\chi\chi} \right)_{\chi\chi} + 5.2256 \left(2\mathcal{U}\mathcal{U}_\tau + \mathcal{U}_\chi \partial_\chi^{-1} \mathcal{U}_\tau \right)_\chi = 0\,. \tag{4.10}$$

It is this equation that we analyse in order to determine the evolution of the wave and mean flow at the Benjamin–Feir transition, and the downshift phenomenon.

4.1. *Heteroclinic connections representing frequency downshifting*

We now solve (4.10), postulating travelling wave solutions of the form

$$\mathcal{U}(X, T) = R(\xi)\,, \quad \text{with} \quad \xi = X - VT\,, \tag{4.11}$$

parametrised by V, where V is the speed of the travelling front. To capture permanent downshifting of the Stokes waves we prescribe the boundary conditions

$$\lim_{\xi \to \infty} R(\xi) = K_1\,, \quad \lim_{\xi \to -\infty} = K_2\,, \qquad K_2 \neq K_1\,. \tag{4.12}$$

These boundary conditions correspond to a pair of asymptotic wavenumbers for the perturbed Stokes waves of the form $k_{1,2} = k_0 + \varepsilon \zeta_1 K_{1,2}$, connecting initial state k_1 (assuming $V > 0$ without loss of generality) to k_2. These assumptions transform (4.10) into an ordinary differential equation, which may be integrated to form a system possessing a quartic potential, with the travelling front now represented by a heteroclinic connection.

The boundary conditions impose that the quartic potential of the ordinary differential equation must possess two repeated roots at K_1 and K_2, and so the system for the frequency

downshifting solution takes the form

$$\left(\frac{\mathrm{d}R}{\mathrm{d}\xi^2}\right)^2 + \frac{\beta_1}{2\beta_3}(R-K_1)^2(R-K_2)^2 = 0\,. \tag{4.13}$$

A comparison between (4.10) and the above gives that the far-field states take one of the following pairs of values:

$$K_{1,2} = \frac{V}{2\beta_1}\left(\beta_2 \pm \sqrt{3\beta_2^2 - 4\beta_1}\right) = (-21.8564 \pm 37.9667)\ V. \tag{4.14}$$

The square root exceeding the leading factor ensures the conjugate states lie on opposite sides of the Benjamin–Feir threshold, and thus connect a Stokes wave which is modulationally unstable to one which is modulationally stable. This is a valuable insight, as this suggests that a transition which leads to $K_2 > K_1$ would be inadmissible owing to the fact that the state it is attempting to connect to is an unstable wavetrain, rather than a uniform wavetrain. Thus, it follows that one should choose $K_2 < 0$ and $K_1 > 0$ on physical grounds to avoid such a scenario. There is an alternative reasoning based on energetics that may also be employed, which is described below in § 5.

Moreover, a secondary insight is that the speed of this transition between bi-asymptotic states is linked to the size of the wavenumber transition, suggesting that larger deviations from the carrier wave will be resolved much more rapidly, in line with what one would expect experimentally. With these boundary conditions and reasoning, this double root corresponds to the jump profile

$$R(\xi) = \frac{1}{2}\ \left[K_1 + K_2 + (K_1 - K_2)\tanh(0.7814\ (K_2 - K_1)\xi)\right]\ . \tag{4.15}$$

The solution family presented here affords novel insight into the frequency downshifting phenomenon from a conservative but dispersive point of view. On the other hand, it is useful to discuss its limitations. Primarily, the solution here presents the connection between two bi-asymptotic states but is unlikely to accurately describe the evolution of the wave as it transitions between them. This is due to the fact that a great number of the higher harmonics and their sidebands contribute to the energy transfer within the wavetrain. This is apparent in the original experiments of Lake *et al.* (1977), where there is a devolution from sideband and harmonic dynamics to a much broader spectral wave evolution.

5. Energetics of frequency downshifting

This analysis of the previous section highlights that two heteroclinic connections are supported by this system, which initially suggests both upshifting and downshifting are permissible. Here we provide some discussion as to how this can be interpreted energetically, leading us to conclude that frequency downshifting arises instead of upshifting. In this discussion, we denote the connection where $k_2 < k_0$ as the lower sideband solution and $k_1 > k_0$ as the upper sideband. These correspond to the bi-asymptotic states of U characterised by $K_2 < 0 < K_1$, respectively.

We begin our discussion with the energy density of the wave, E, under the action of the jump solution (4.15). By comparing lower and upper sideband wavenumbers we are able to show from (A1) that the energy density of the sidebands is related to the energy density of the carrier wave, E_0, to leading order via

$$E_{1,2} = E_0 - \varepsilon\sqrt{E}\ \omega_0''\mathscr{M}_1 K_{1,2} + \mathcal{O}\left(\varepsilon^2\sqrt{E}, \varepsilon E\right). \tag{5.1}$$

Thus, it is clear that $E_1 < E_0 < E_2$ and so more energy is passed to the lower sideband than to the upper sideband under the jump mechanism. This is in line with experimental (e.g. Lake *et al.* 1977; Melville 1982) and theoretical (e.g. Bryant 1982) observations. The primary driver of this energy exchange is the mean-flow effect, suggesting the mechanism for the sideband asymmetry is indeed a mean-flow aspect of the problem rather than the wave. Additionally, the energy of the lower sideband as $T \to \infty$ under this mechanism exceeds that of the carrier wave, as also seen in the aforementioned studies. These facts together suggest that there is an overall shift in energy downwards in the spectrum over long time, and thus the spectral peak moves from the carrier wavenumber to that of the lower sideband.

The energy density alone does not, however, indicate whether the upshift or downshift is ultimately selected by the system but can be resolved by looking at the total wave energy. Recall the definition of wave energy for the water-wave problem (Whitham 2011):

$$\mathscr{E} = \frac{1}{2}(h_0 + b)\left(u + \frac{E}{c_0(h_0 + b)}\right)^2 + \frac{1}{2}g(h_0 + b)^2 + E\,. \tag{5.2}$$

Let us denote the wave energy of the carrier wave by $\mathscr{E}_0$. Then to leading order the energy of the upper and lower sidebands is

$$\mathscr{E}_{1,2} = \mathscr{E}_0 - \varepsilon\sqrt{E}\omega_0'' K_{1,2}\left[gh_0\mathscr{M}_2 + \mathscr{M}_1\right] + \mathcal{O}\left(\varepsilon E, \varepsilon^2\sqrt{E}, \varepsilon b\right), \tag{5.3}$$

with $\mathscr{M}_2$ defined in (A2) of Appendix A. It follows from evaluating the above at the Benjamin–Feir stability transition that $\mathscr{E}_2 < \mathscr{E}_0 < \mathscr{E}_1$ and therefore indicates that the downshifting is the most energetically viable state of the three. This affords a concrete explanation as to why downshifting may occur in the absence of viscosity: by downshifting, the Stokes wave is able to lower its wave energy and restabilise itself.

5.1. *Commentary on recurrence of the Stokes wave solution*

In the majority of previous studies into the phenomena of frequency downshifting, it is argued that the shift in spectral peak to lower frequency/wavenumber is a transient process and the system undergoes Fermi–Pasta–Ulam–Tsingou recurrence. This was primarily reported in Yuen & Lake (1982) and Bryant (1982) with the notion being refined in Lo & Mei (1985) and Hara & Mei (1991), which was obtained by perturbing the carrier wave by the most (and only) unstable wave mode in the nonlinear Schrödinger or Dysthe equation. However, once further sideband modes became unstable recurrence behaviour was lost completely and much more complicated dynamics occurs (see the commentary of § 6 of Lo & Mei (1985) for their discussion on the matter). It transpires that this is also true if waves other than integer harmonics are initially excited within the system, where the wave–wave interactions cease to be closed, as in Zakharov equations (Onorato *et al.* 2002; Janssen 2003). We note that the heteroclinic connection we have proposed does not necessarily link a wave to its harmonic and thus we do not expect our interactions to be closed in the same way within our numerical procedures in § 6). This explains why, in the simulations within our paper regarding the presence of the heteroclinic wavenumber connection (4.15), we do not observe any recurrence behaviour within the simulations.

On the other hand, it is the case that the phase dynamics, in the neighbourhood of the Benjamin–Feir transition, can capture recurrence behaviour. Primarily, oscillating solutions (corresponding to a back-and-forth transition between and initial and sideband wavenumber) can be obtained when the quartic potential associated with the travelling wave solutions of (4.10) has simple roots (Johnson 2009; Kamchatnov *et al.* 2012). As with the Gardner and mKdV equations, these can be either cnoidal or dnoidal solutions

depending on which roots possess a valid connecting trajectory. It is more likely to be the former of these families responsible for the recurrence observed elsewhere, as the energy exchanges between modes are observed to have deeper troughs and sharper peaks; see, for example, figure 3 in Yuen & Ferguson Jr (1978) or figure 13(*a*) in Lo & Mei (1985).

The use of pseudo-spectral methods within this paper (and thus periodic boundary conditions) raises the question of numerical feasibility of the phase dynamical solution outlined in § 4.1, as this would not be permissible in these numerical treatments as its boundary conditions would violate the periodicity required for spectral methods. This periodicity is not present experimentally, since this corresponds to an annular set-up, and instead the energy is absorbed at the end of the tank and not redistributed within the wavetrain at later times. Thus, it is no surprise that pseudo-spectral numerical and Fourier-based approaches have thus far failed to explain conservative permanent frequency downshifts observed in experiments. Moreover, the mechanism for dissipation, thought to be wavebreaking, is not observed until the wave steepness exceeds a certain threshold and the dissipative picture fails to adequately explain the presence of permanent downshifts in less steep waves.

An intermediary between these periodic solutions and the jump profile is the tabletop solitary wave solution, arising when the potential possesses a double root and the remaining two roots are close to equal. In the context of phase dynamics, it represents a temporary shift in the wavenumber of a similar form to the jump solution discussed in § 4.1 that eventually undergoes an inverse jump transition to the original wavenumber. Such solutions respect the periodicity requirement so long as the width of the tabletop solitary wave is less than the spatial domain. As such, one may repeat the travelling wave analysis for one repeated root and two that are 2δ apart:

$$\left(\frac{\mathrm{d}R}{\mathrm{d}\xi^2}\right)^2 + \frac{\beta_1}{2\beta_3}(R-K^\infty)^2(R-K^0+\delta)(R-K^0-\delta) = 0\,. \tag{5.4}$$

Here K^∞ represents the far-field value of the solution and K^0 denotes the limiting value of the temporary wavenumber transition. The temporary downshifting solution corresponds to the case in which $K^0 < K^\infty$, to which we restrict our discussion. Comparisons with (4.10) give that these take one of the following pairs of values:

$$\begin{aligned} K^\infty &= \frac{V}{2\beta_1}\left(\beta_2 + \sqrt{3\beta_2^2 - 4\beta_1 - 2\left(\frac{\beta_1\delta}{V}\right)^2}\right) \\ &= \left(-21.8564 + \sqrt{1441.4706 - \frac{1}{2}\left(\frac{\delta}{V}\right)^2}\right)V, \\ K^0 &= \left(-21.8564 - \sqrt{1441.4706 - \frac{1}{2}\left(\frac{\delta}{V}\right)^2}\right)V. \end{aligned} \tag{5.5}$$

Thus, one may obtain the positive-polarity solitary wave solution (Kamchatnov *et al.* 2012):

$$R = K^\infty + \frac{(K^0-K^\infty)^2 - \delta^2}{K^0 - K^\infty - \delta + \delta\cosh^2(0.7814\sqrt{(K^0-K^\infty)^2-\delta^2}\,\xi)}\,. \tag{5.6}$$

As the parameter $\delta < 0$ approaches zero, the solitary wave becomes the previously mentioned tabletop solitary wave with amplitude close to $K^0 - K^\infty$. This profile can be tested in numerical simulations in order to deduce its stability and robustness in the water-wave problem via the use of reduced modelling. Such discussion can be found in section § 6.

6. Numerical validation of the phase dynamics solutions

In order to verify the theoretical conclusions, arrived at from the phase dynamics analysis, we resort to a numerical investigation of a system representative of the water-wave problem. We use the simplest water-wave model which contains the essential wave dynamics coupled to the mean flow, namely the Benney–Roskes system in (2.32)–(2.34). The Benney–Roskes system possesses the same characteristic features, elliptic–hyperbolic transition and phase dynamical picture as the full water-wave problem in the case where $\mu,\ \tau$ in (2.5) are held fixed. Towards this end, we expect the tabletop solitary wave solution (5.6) to remain close to an exact solution within the Benney–Roskes system.

To initialise the simulations, we use the solution (5.6) in dimensional form and construct A, B and W according to (A3) (accounting for the fact that the smallness of a and b has been factored out via ϵ). In terms of the Benney–Roskes variables, the initial condition is constructed as

$$A = \sqrt{|A_0|^2 - 0.9171\tilde{\varepsilon}U}\,, \qquad B = B_0 + 0.8220\tilde{\varepsilon}U\,, \qquad W = W_0 + 3.4527\tilde{\varepsilon}U\,, \quad (6.1)$$

where U is taken to be the tabletop solution. The small parameter $\tilde{\varepsilon} = \varepsilon/\epsilon$ is a reduced small parameter which accounts for the small scale for which the Benney–Roskes system is operational, ϵ. For simplicity we choose $|A_0|^2 = 1$ and $B_0 = W_0 = 0$. This tabletop solution's width (via choice of δ) is chosen so that the added perturbation contributes no additional mass to the Stokes wave to leading order on a principal domain of length L (typically, 80 wavelengths to ensure the tabletop is sufficiently flat), so that

$$\int_{-L/2}^{L/2} U(\xi, T)\,\mathrm{d}\xi = 0. \quad (6.2)$$

We then inflate our computational domain by some factor of order 10, depending on the simulation time and distance from the Benjamin–Feir threshold, to ensure recursion does not occur in our numerical solution as discussed in § 5.1. Later wavenumber properties are then computed on the principal domain of length L. We choose the reference wavenumber k_0 to be unity and control the distance to the Benjamin–Feir threshold via the choice of $h_0 \in [1.3, 1.3626]$ to ensure hyperbolicity of the underlying dynamics but to remain close to the modulation instability threshold. The smallness parameter of the Stokes waves is chosen as $\epsilon \sim 10^{-1}$ to align with typical experimental values for the steepness, and we note that this latter choice impacts simulation times due to its presence within the amplitude's evolution. We set $\varepsilon \sim \epsilon^2$ so that $\tilde{\varepsilon} \sim \epsilon$ in order to remain in the domain of asymptotic validity of the phase dynamics. For the time integration, we simulate in a periodic domain using an exponential time differencing scheme with Runge–Kutta timestepping of order 4 (Cox & Matthews 2002) with the stability modifications outlined within Kassam & Trefethen (2005). This numerical scheme has been verified in a number of ways, including verification that the system conserves mass to 10^{-3} % accuracy, that it admits the expected soliton solution when restricted to only the envelope equation (2.32) with $W = B = 0$ and that when restricted to the shallow-water components (2.33) and (2.34) with $A = 0$ the solution generates two profiles which move at the characteristic speeds $-c_g \pm \sqrt{gh_0}$.

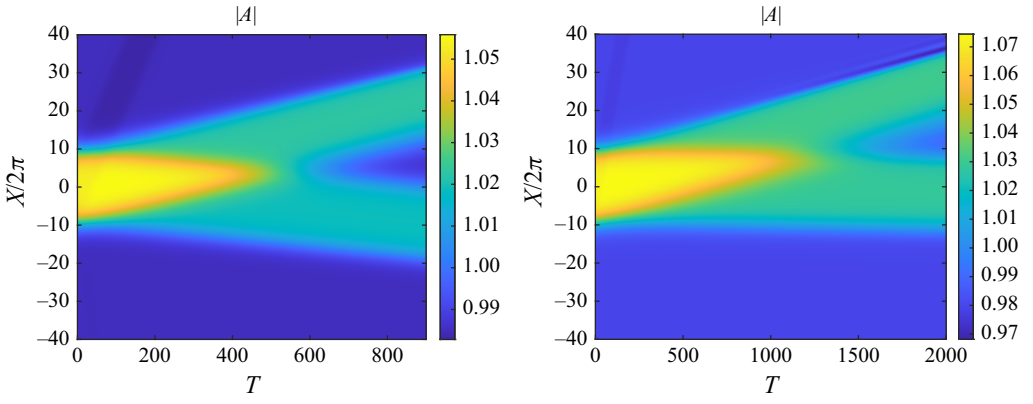

Figure 1. Space–time plots of the evolution of the wave envelope $|A|(X, T)$ for $k_0h_0 = 1.3$ (left) and $k_0h_0 = 1.36$ (right). The initial tabletop splits into four components, each associated with one of the characteristics speeds of (2.32)–(2.34).

Momentum is not conserved in the Benney–Roskes system, as we discuss later within this section in relation to downshifting.

A representative example of the outcome of these simulations appears in figure 1. What is observed is that the initial tabletop lump splits into four components, two associated with the long-wave speed of the shallow-water component and two associated with the wave's group velocity. The latter two components emerge much later than the former as one would expect, and the amplitudes of these modes differ owing to the higher-order terms present in the phase dynamical ansatz. All profiles maintain their general form within the simulation times, although one should note that the profiles associated with the group velocity can develop dispersive shocks at their leading edge if the initial data are large enough. Whilst this is likely indicative that the initial condition is outside the remit of the validity of the phase dynamics, this shock formation does not significantly impact the observations related to the wavenumber discussed below. In fact, this appears to be more reflective of the experimental observations of downshifting observed by Lake *et al.* (1977), where the transition occurred via a modulation–demodulation cycle.

We may also visualise the impact of these results on the original Stokes wave, which is done by reconstructing the free surface according to

$$\eta = \epsilon A \mathrm{e}^{1k_0X/\varepsilon} + \text{c.c.} + \varepsilon^2 B + \cdots, \tag{6.3}$$

where we have focused on the leading-order wave–mean-flow effects in this reconstruction. These can be seen in figure 2, which highlights that the amplitude increase comes together with a drop in the mean fluid depth. Further, one can observe the presence of a slight change in wavenumber either side of the transition. This confirms the theoretical observations of this paper that a downshift in wavenumber comes with an amplitude increase and mean fluid level decrease (cf. (A3)).

We may also use these simulations to investigate the behaviour of the wavenumber of the Stokes wave. In the framework of the Benney–Roskes system, this relates to the full surface wave's wavenumber k via

$$k_{wave} = k_0 + \epsilon\, k_{BR}, \tag{6.4}$$

where k_{BR} denotes the wavenumber extracted from the simulation. There are two key approaches we take to extract this perturbative wavenumber within the simulations.

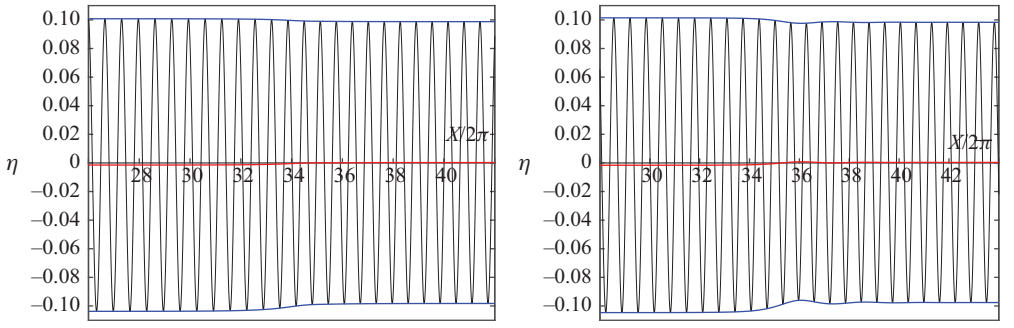

Figure 2. Visualisation of the free surface η reconstructed from the numerical solution of the Benney–Roskes system at the final simulation time for the simulations of figure 1.

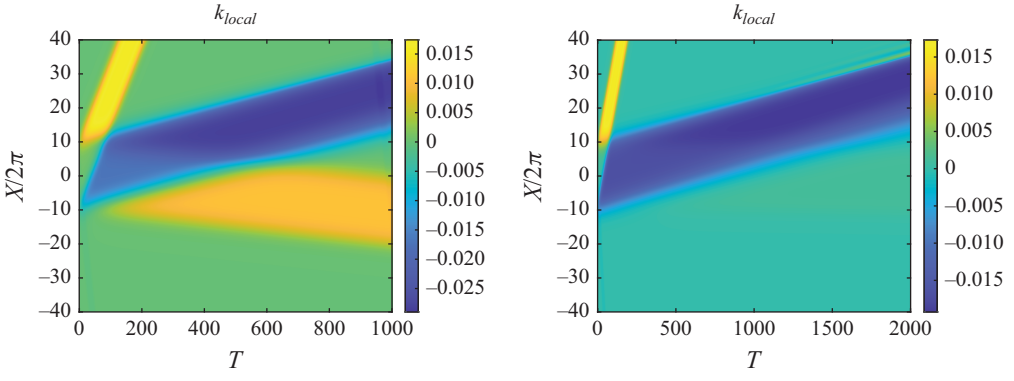

Figure 3. Plots of the local wavenumber k_{local}, as defined in (6.5), associated with the profiles in figure 1.

Our first approach is to extract the local wavenumber behaviour of the wave amplitude via the definition

$$k_{BR} = k_{local}(X, T) = \mathrm{Im}\left[\partial_X \ln\left(\frac{A}{|A|}\right)\right], \tag{6.5}$$

where Im indicates that the imaginary part is taken. An example of this extracted local wavenumber for a simulation appears in figure 3. We observe that there are three significant contributors to the local wavenumber change, two from the group velocity modes and one from the long-wave mode. This latter mode emerges first and corresponds to an increase in wavenumber, and although this is not associated with the wavenumber transitions we intend to study it is not unexpected as this will correspond to another seemingly linear phase dynamic (cf. § 3). Of the two modes associated with the group velocity, the larger-amplitude right-moving mode is responsible for the decrease in wavenumber and is significantly larger than the increase in local wavenumber of the other mode.

The second approach we take to determine wavenumber behaviour, particularly the emergent wavenumber behaviour for the entire wavetrain solution, is to study the spectral mean, following Carter *et al.* (2019). It is defined by

$$k_{BR} = k_m(T) = \frac{i\int AA_X^* - A^*A_X \,\mathrm{d}X}{2\int |A|^2 \,\mathrm{d}X} \equiv \frac{\int k|\hat{A}|^2 \,\mathrm{d}k}{\int |\hat{A}|^2 \,\mathrm{d}k}, \tag{6.6}$$

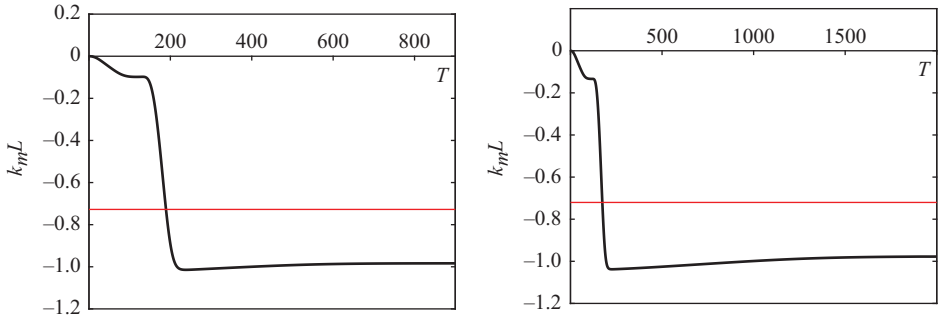

Figure 4. Spectral mean of the wavenumbers associated with the profiles in figure 1 as a function of time. The red line denotes the arithmetic mean of the long-time local wavenumber plateau values.

where $\hat{A}(k, T)$ is the Fourier transform of the wave amplitude A. Whilst the momentum $\mathscr{P} = \int k|\hat{A}|^2 \, \mathrm{d}k$ is conserved in the dynamics of the nonlinear Schrödinger equation, it is not necessarily conserved under Benney–Roskes dynamics as

$$\frac{\mathrm{d}\mathscr{P}}{\mathrm{d}T} = -2\left(k_0 W_X + \frac{gk_0^2 - \omega_0^4}{2g\omega_0} B_X\right)|\hat{A}|^2. \tag{6.7}$$

It is worth noting that the right-hand side of the above expression is not sign definite, and so upshifting of the spectral mean is also permitted. We also note that the (total) wave mass (i.e. the denominator of (6.6)) is conserved under both the nonlinear Schrödinger dynamics and the Benney–Roskes dynamics, but the mass on the domain that we examine, namely the original domain of length L, the mass will decrease as the long-wave modes leave this portion of the domain. This causes the mass in this domain of interest to decrease but it does so almost negligibly. This lack of conservation of spectral mean permits the spectral mean to change over the wavetrain's evolution, and we find that it decreases as depicted in figure 4. It depicts what is typical of a simulation with the prescribed set-up: the wavenumber drops significantly as the long-wave modes propagate out from the initial tabletop and subsequently out of the domain of interest, before slowly increasing (i.e. a minor upshift, as permitted by (6.7)) to a negative asymptotic value. This value is reasonably close to the arithmetic mean of the local wavenumbers of each tabletop solution, suggesting that the spectral mean is the result of these wavenumber shifts. It confirms, however, that the tabletop solution is the source of the negative spectral mean value and that it remains stable over the course of its propagation.

What the Benney–Roskes system also allows us to do is to explore the elliptic (i.e. modulationally unstable) regime, unlike the phase dynamical description. What we do find, despite the phase dynamical description being invalid here, is that the same trend of frequency downshifting persists and in its initial stages follows the hyperbolic regime with an example appearing in figure 5. As the modulation instability sets in, it works to improve the downshift substantially and decreases the wavenumber much further than the modulationally stable wavetrain close to threshold. We also observe that the transfer of energy in the power spectrum biases lower wavenumbers in line with the the observations from experiments (Lake *et al.* 1977; Melville 1982; Su *et al.* 1982). We re-emphasise that there are no dissipative effects here – this bias towards lower wavenumbers in the numerical simulation is entirely mean-flow-driven. It does, however, remain an open question whether the wave profiles within these simulations become steep enough to break and thus for dissipation to play a role in this regime, but these simulations show that this is

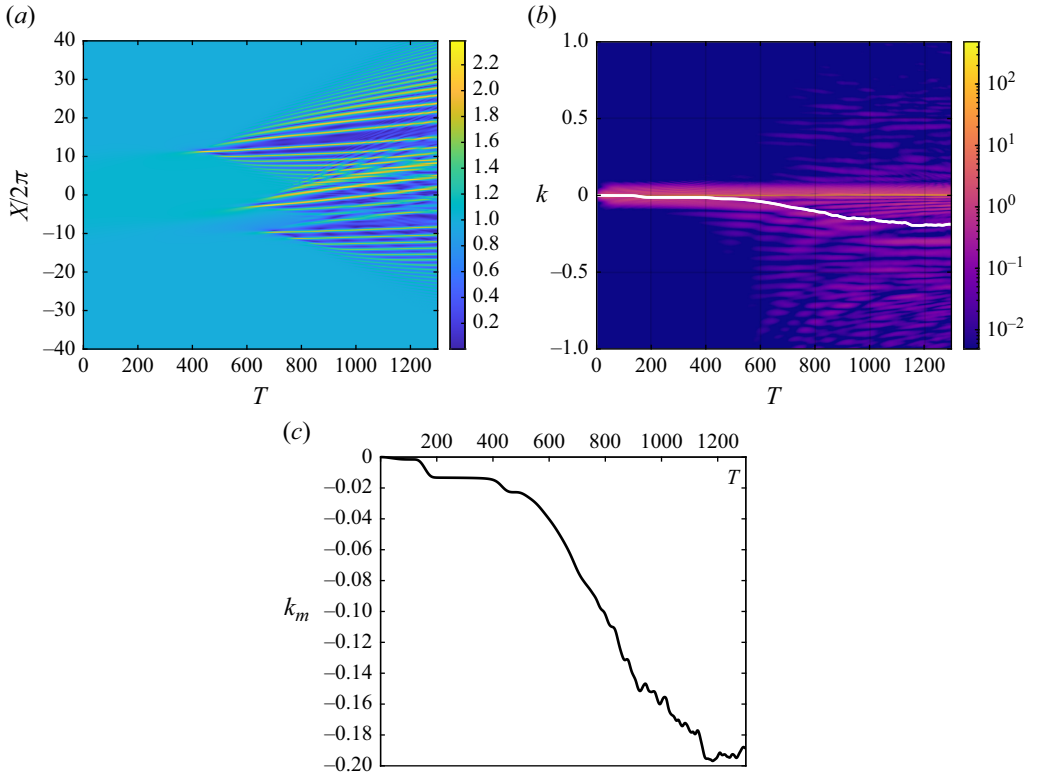

Figure 5. A numerical simulation for $k_0h_0 = 1.4$, showing the amplitude (*a*), power spectral density (*b*) and spectral mean wavenumber (*c*). The spectral mean wavenumber is marked with a white line on the power spectral density in (*b*).

not required for the downshifting phenomena in the modulationally unstable regime. What we do not see in this case is recurrence or restabilisation, instead seeing the formation of a soliton train which initially forms at the edges of the splitting tabletop solitary wave and expands over the simulation time.

7. Concluding remarks

This paper has introduced a mechanism for water waves to undergo a permanent frequency downshift without dissipative effects. Mathematically, it is due to a local loss of genuine nonlinearity arising at the Benjamin–Feir transition that introduces higher-order effects that support front profiles for the wavenumber's evolution. Energetically, it occurs because of a decrease in energy which restabilises the Stokes wave. This energetic perspective helps to reinforce the observations that the energy exchange to the lower sideband is much higher than that to upper sidebands. This paper highlights that these effects are due to mean-flow effects present in the problem. As a consequence, one of the key conclusions of this paper is that the interplay between wave motion and mean flow is important and should be more carefully considered in the water-wave problem. Our study here suggests that slaving the mean-flow effects to the wave motion, either as part of a reduction to nonlinear Schrödinger (Ablowitz & Segur 1981; Johnson 1997) or the earlier treatments of the water-wave problem from a modulation perspective (Whitham 1967, 2011), omits important aspects of the dynamics of Stokes waves.

This paper has demonstrated numerically that downshifting is the wave's preferred outcome in the neighbourhood (and in the case of the elliptic regime, the presence of) modulation instability. It has shown this preference for downshifting via a reduction of the full water-wave problem that accounts for both wave and mean-flow evolution in space and time, the Benney–Roskes system, revealing behaviour absent from amplitude-only models and again emphasising that these outcomes must be attributed to the wave–mean-flow interplay of the problem. The numerical results also underscore that it is possible to have this downshift be permanent and not part of a recurrence cycle, as previously argued to be the only possibility in conservative systems (Lo & Mei 1985). Whilst this is a simulation of an approximation of the full water-wave problem, it provides an important first step in the verification of this phenomenon in the full water-wave problem. The requirement of spatiotemporal evolution to observe the downshifting phenomenon suggests that solvers that seek minimiser (such as the scheme of Ablowitz, Fokas & Musslimani (2006)) may not be the appropriate way to validate this phenomenon, and instead one should utilise either conformal (Dyachenko, Zakharov & Kuznetsov 1996; Choi & Camassa 1999) or canonical (Craig & Sulem 1993) formulations to explore the phenomenon within the full Euler equations.

We re-emphasise that, whilst the explanation for downshifting without reliance on dissipation is an important step forward in our understanding of the phenomenon, dissipation remains one possible (and provably successful) mechanism for decreases in spectral peaks (Carter *et al.* 2019). Particularly, the dissipative description is valid deep into the elliptic regime, well outside of the transition regime to which the phase dynamical description of this paper is applicable. An important future avenue for study will be to compare the interplay of these effects and in which regimes one effect may dominate over the other and to the degree to which it does so.

It is worth noting that this study of mean-flow-driven downshifting highlights that upshifting of the Stokes wave is also a possibility, highlighted by the form of the heteroclinic connection as well as the connection to the Benney–Roskes equation. Particularly, (6.7) demonstrates that the spectral mean may increase in some instances, as has been reported experimentally (Ma *et al.* 2012). The energetic arguments of § 5, which suggest long-term downshifting, only hold in the hyperbolic case and cease to be valid in the elliptic regime. This suggests upshifting is only possible once the Benjamin–Feir instability is operational, but this should be verified as part of further studies into this phenomenon.

The assumption of gravity waves is important here, as it ensures that $\omega_0'' \neq 0$ for any choice of k and thus ensures the non-degeneracy of the phase dynamics. The inclusion of capillary effects introduces a new modulation stability boundary at points where $\omega_0'' = 0$, and such points cause every coefficient in (3.9) to become zero. To rebalance the phase dynamics in this case, one must include higher-order dispersive effects in addition to the considerations made for the scenario of this paper. The result is a fully extended version of the two-way Boussinesq equation which supports localised solutions as well as fronts.

The mechanism proposed here is universal in that it does not rely on a particular governing equation, just on the fact that the equations are generated by a Lagrangian and there exists a multi-parameter family of periodic or multi-periodic travelling waves, with parameter values at which two characteristics coalesce, and furthermore the nonlinearity in the re-modulation is cubic. Indeed, generalisations of the water-wave problem (inclusion of surface tension, variable density, electromagnetic fields, etc.), at both finite amplitude and weakly nonlinear limit, would be settings where the above scenario is likely to occur.

Although downshifting has been shown to be the only energetically viable result in the gravity water-wave problem at the threshold of modulation instability, upshifts are

also theoretically possible in other physical systems. For example, Whistler waves in the magnetosphere may undergo a downshift or an upshift depending on whether they are travelling parallel or orthogonal to the background magnetic field (Omura, Katoh & Summers 2008; Omura 2021; Ratliff & Allanson 2023). The analysis performed here is likely to explain when this is permissible and will be due to how the amplitude varies with the mean-flow element (which for plasmas takes the role of velocity and number density perturbations), in comparison with the principal change in the wavenumber and frequency.

Acknowledgements. D.J.R. would like to thank the participants of the *Dispersive Hydrodynamics* programme, especially P. Sprenger and P. Milewski, for their invaluable discussions throughout the development of this work.

Funding. The authors would like to thank the Isaac Newton Institute for Mathematical Sciences for support and hospitality during the programme *Dispersive Hydrodynamics* when work on this paper was undertaken. This work was supported by EPSRC grant number EP/R014604/1.

Declaration of interest. The authors report no conflict of interest.

Appendix A. Effect of mean velocity on the amplitudes *a* and *b*

The perturbative impact on the amplitude and mean flow of the Stokes wave, in the neighbourhood of fixed values (a_0, b_0), is given in this appendix. Using the definitions (2.12), (2.25) and (B2), we can show that the leading-order contributions to their change is

$$\begin{aligned} a &= a_0 + \frac{gh_0 + B_0\omega_0'}{c_0 h_0 \Delta_W}\varepsilon\zeta_2 U + \mathcal{O}\big(\varepsilon\sqrt{E}, \varepsilon^2\big)\,, \\ b &= b_0 - \frac{1}{\omega_0 \Delta_W}\left(\omega_2^0\omega_0' + \frac{B_0 k}{c_0 h_0}\right)\varepsilon\zeta_2 U + \mathcal{O}\big(\varepsilon\sqrt{E}, \varepsilon^2\big)\,, \end{aligned} \tag{A1}$$

where ζ_2 is the second component of the eigenvector $\boldsymbol{\zeta}$ in (2.21). This expansion highlights that the primary effect on the Stokes waves arises from the mean-flow element of the problem, evident from the appearance of ζ_2, as opposed to being driven by the wave itself. The expressions preceding the perturbation U represent recurring factors within the analysis, and so it is convenient to define the two quantities

$$\mathscr{M}_1 = \frac{gh_0 + B_0\omega_0'}{c_0 h_0 \Delta_W} < 0\,, \qquad \mathscr{M}_2 = -\frac{1}{\omega_0 \Delta_W}\left(\omega_2^0\omega_0' + \frac{B_0 k}{c_0 h_0}\right) > 0\,. \tag{A2}$$

These quantities arise due to the variations of the wave amplitude and bulk flow due to the mean-flow effects and are important in characterising the impact of these effects on the dynamics of the wave. Evaluating these perturbations to the wave amplitude and bulk flow at the Benjamin–Feir transition, one finds

$$a = a_0 - 0.9171\varepsilon U + \mathcal{O}\big(\varepsilon\sqrt{E}, \varepsilon^2\big), \qquad b = b_0 + 0.8220\varepsilon U + \mathcal{O}\big(\varepsilon\sqrt{E}, \varepsilon^2\big). \tag{A3}$$

As $\zeta_1 > 0$ at the transition, one can infer that increases in the wavenumber, corresponding to positive U, result in a decrease of amplitude and a rise (drop) in mean level, and vice versa. This is in line with the experimental observations of Lake *et al.* (1977). We may also use this information to infer the stability of the Stokes wave by assessing how the non-dimensional depth kh changes near this transition. To leading order, this is

$$kh = kh_0 + 2.0829\varepsilon U + \mathcal{O}\big(\varepsilon\sqrt{E}, b, \varepsilon^2\big)\,. \tag{A4}$$

As expected, the states which increase the wavenumber also increase kh, but do so at a faster rate than the changes in the mean level that would otherwise balance it out.

Appendix B. Explicit expressions for matrix pencil entries

Explicit expressions for the entries of the matrix pencil $\mathbf{E}(c)$ defined in (2.21) are given here:

$$\begin{aligned}
E_{11} &= \frac{g(c-c_g)^2}{\omega_0^2 \Delta_W} + \left[\frac{\omega_0''}{\omega_0} + \frac{c-c_g}{\omega_0}\left(\frac{(c-c_g-2\omega_0')}{\omega_0} + \frac{2}{c_0 h_0 \Delta_W}(B_0\mu' - g\tau')\right)\right] E \\
&\quad - \frac{2g(c-c_g)}{\omega_0 \Delta_W}\mu' kb, \\
E_{12} &= -\frac{(c-c_g)(gh_0 + B_0(c-u))}{c_0^2 k h_0 \Delta_W} \\
&\quad + \left[\frac{c-c_g-\omega_0'+c_0}{c_0^2 k} + \frac{(gh_0 + B_0(c-u))}{c_0 h_0 \Delta_W}\tau' - \frac{1}{\Delta_W}\left(\frac{kB_0}{c_0 h_0} + \omega_2^0(c-u)\right)\mu'\right] E \\
&\quad + \frac{(gh_0 + B_0(c-u))}{c_0 h_0 \Delta_W}\mu' b, \\
E_{22} &= \frac{gh_0 + 2B_0(c-u) + B_0^2}{c_0^2 h_0 \Delta_W} - \frac{\omega_2(gh_0 - (c-u)^2)}{\omega_0 \Delta_W} + b - \frac{E}{c_0^2}.
\end{aligned} \tag{B1}$$

This matrix has a right eigenvector associated with the characteristic (2.25) defined by $\mathbf{E}(c)\boldsymbol{\zeta} = 0$. It can be expanded for small amplitude to give

$$\begin{aligned}
\boldsymbol{\zeta} &= \begin{pmatrix}\zeta_1 \\ \zeta_2\end{pmatrix} = \pm\sqrt{\omega_0'' \omega_2^{eff}}\,\boldsymbol{\chi} \\
&\quad + \sqrt{E}\left[C_2\boldsymbol{\chi} - \begin{pmatrix} \dfrac{B_0\omega_0''\omega_2^{eff}}{c_0 h_0 \Delta_W} + \dfrac{\omega_0'}{c_0} - 1 + \dfrac{1}{\Delta_W}\left(\omega_2^0\omega_0' + \dfrac{kB_0}{c_0 h_0}\right)\mu' - \dfrac{k(B_0\omega_0' + gh_0)}{h_0 \Delta_W}\tau' \\ \omega_0''\left(1 + \frac{g\omega_2^{eff}}{\omega_0 \Delta_W}\right) \end{pmatrix}\right] \\
&\quad \pm E\left[C_3\boldsymbol{\chi} + \sqrt{\omega_0''\omega_2}\left(\begin{pmatrix}\frac{1}{c_0} \\ 0\end{pmatrix} + \frac{2C_2}{\Delta_W}\begin{pmatrix}\mu \\ -\frac{g}{\omega_0}\end{pmatrix}\right)\right] + \mathcal{O}(E^{3/2}),
\end{aligned} \tag{B2}$$

with

$$\boldsymbol{\chi} = -\frac{1}{c_0 h_0 \Delta_W}\begin{pmatrix} gh_0 + B_0\omega_0' \\ 0 \end{pmatrix}, \tag{B3}$$

where C_3 is a further term in the amplitude expansion of the characteristic. It is not given here as it does not contribute to the analysis at the orders considered.

References

Ablowitz, M.J., Fokas, A.S. & Musslimani, Z.H. 2006 On a new non-local formulation of water waves. *J. Fluid Mech.* **562**, 313–343.

Ablowitz, M.J. & Segur, H. 1981 *Solitons and the Inverse Scattering Transform*. SIAM.

Benjamin, T.B. 1967 Instability of periodic wavetrains in nonlinear dispersive systems. *Proc. R. Soc. Lond. A* **299** (1456), 59–76.

Benjamin, T.B. & Feir, J.E. 1967 The disintegration of wave trains on deep water part 1. theory. *J. Fluid Mech.* **27** (3), 417–430.

Benney, D.J. & Roskes, G.J. 1969 Wave instabilities. *Stud. Appl. Maths* **48** (4), 377–385.

Berti, M., Maspero, A. & Ventura, P. 2023 Benjamin–Feir instability of Stokes waves in finite depth. *Arch. Ration. Mech. Anal.* **247** (5), 91.

Berti, M., Maspero, A. & Ventura, P. 2024 Stokes waves at the critical depth are modulationally unstable. *Commun. Math. Phys.* **405** (3), 56.

Bridges, T.J. 2014 Emergence of dispersion in shallow water hydrodynamics via modulation of uniform flow. *J. Fluid Mech.* **761**, R1.

Bridges, T.J. & Donaldson, N.M. 2006 Secondary criticality of water waves. Part 1. Definition, bifurcation and solitary waves. *J. Fluid Mech.* **565**, 381–417.

Bridges, T.J. & Mielke, A. 1995 A proof of the Benjamin–Feir instability. *Arch. Ration. Mech. Anal.* **133** (2), 145–198.

Bridges, T.J. & Ratliff, D.J. 2017 On the elliptic-hyperbolic transition in Whitham modulation theory. *SIAM J. Appl. Maths* **77** (6), 1989–2011.

Bridges, T.J. & Ratliff, D.J. 2021 Nonlinear theory for coalescing characteristics in multiphase Whitham modulation theory. *J. Nonlinear Sci.* **31** (1), 7.

Bridges, T.J. & Ratliff, D.J. 2022 Reappraisal of Whitham's 1967 theory for wave-meanflow interaction in shallow water. *Wave Motion* **115**, 103050.

Bryant, P.J. 1982 Modulation by swell of waves and wave groups on the ocean. *J. Fluid Mech.* **114**, 443–466.

Carter, J.D. & Govan, A. 2016 Frequency downshift in a viscous fluid. *Eur. J. Mech. B/Fluids* **59**, 177–185.

Carter, J.D., Henderson, D. & Butterfield, I. 2019 A comparison of frequency downshift models of wave trains on deep water. *Phys. Fluids* **31** (1), 013103.

Chalikov, D. 2007 Numerical simulation of the Benjamin–Feir instability and its consequences. *Phys. Fluids* **19** (1), 016602.

Chalikov, D. 2012 On the nonlinear energy transfer in the unidirected adiabatic surface waves. *Phys. Lett. A* **376** (44), 2795–2798.

Choi, W. & Camassa, R. 1999 Exact evolution equations for surface waves. *J. Engng Mech.* **125** (7), 756–760.

Cox, S.M. & Matthews, P.C. 2002 Exponential time differencing for stiff systems. *J. Comput. Phys.* **176** (2), 430–455.

Craig, W. & Sulem, C. 1993 Numerical simulation of gravity waves. *J. Comput. Phys.* **108** (1), 73–83.

Creedon, R.P. & Deconinck, B. 2023 A high-order asymptotic analysis of the Benjamin–Feir instability spectrum in arbitrary depth. *J. Fluid Mech.* **956**, A29.

Deconinck, B. & Oliveras, K. 2011 The instability of periodic surface gravity waves. *J. Fluid Mech.* **675**, 141–167.

Dias, F. & Kharif, C. 1999 Nonlinear gravity and capillary-gravity waves. *Annu. Rev. Fluid Mech.* **31** (1), 301–346.

Doelman, A., Sandstede, B., Scheel, A. & Schneider, G. 2009 *The Dynamics of Modulated Wave Trains*. American Mathematical Soc.

Dyachenko, A.I., Zakharov, V.E. & Kuznetsov, E.A. 1996 Nonlinear dynamics of the free surface of an ideal fluid. *Plasma Phys. Rep.* **22** (10), 829–840.

Dysthe, K.B., Trulsen, K., Krogstad, H.E. & Socquet-Juglard, H. 2003 Evolution of a narrow-band spectrum of random surface gravity waves. *J. Fluid Mech.* **478**, 1–10.

Gear, J.A. & Grimshaw, R. 1983 A second-order theory for solitary waves in shallow fluids. *Phys. Fluids* **26** (1), 14–29.

Hara, T. & Mei, C.C. 1991 Frequency downshift in narrowbanded surface waves under the influence of wind. *J. Fluid Mech.* **230**, 429–477.

Hasimoto, H. & Ono, H. 1972 Nonlinear modulation of gravity waves. *J. Phys. Soc. Jpn.* **33** (3), 805–811.

Hruslov, E.J. 1976 Asymptotics of the solution of the Cauchy problem for the Korteweg-de Vries equation withinitial data of step type. *Maths USSR* **28** (2), 229–248.

Huang, N.E., Long, S.R. & Shen, Z. 1996 The mechanism for frequency downshift in nonlinear wave evolution. *Adv. Appl. Mech.* **32**, 59–117C.

JANSSEN, P.A.E.M. 2003 Nonlinear four-wave interactions and freak waves. *J. Phys. Oceangr.* **33** (4), 863–884.

JOHNSON, M.A. 2009 Nonlinear stability of periodic traveling wave solutions of the generalized Korteweg–de Vries equation. *Siam J. Math. Anal.* **41** (5), 1921–1947.

JOHNSON, R.S. 1977 On the modulation of water waves in the neighbourhood of $kh \approx 1.363$. *Proc. R. Soc. Lond. A* **357**, 131–141.

JOHNSON, R.S. 1997 *A Modern Introduction to the Mathematical Theory of Water Waves*. Cambridge University Press.

KAKUTANI, T. & MICHIHIRO, K. 1983 Marginal state of modulational instability – note on Benjamin–Feir instability. *J. Phys. Soc. Jpn.* **52** (12), 4129–4137.

KAMCHATNOV, A.M., KUO, Y.-H., LIN, T.-C., HORNG, T.-L., GOU, S.-C., CLIFT, R., EL, G.A. & GRIMSHAW, R.H.J. 2012 Undular bore theory for the Gardner equation. *Phys. Rev. E* **86** (3), 036605.

KASSAM, A.-K. & TREFETHEN, L.N. 2005 Fourth-order time-stepping for stiff pdes. *SIAM J. Sci. Comput.* **26** (4), 1214–1233.

KORTEWEG, D.J. & DE VRIES, G. 1895 On the change of form of long waves advancing in a rectangular canal, and on a new type of long stationary waves. *Lond. Edinburgh Philos. Mag. J. Sci.* **39** (240), 422–443.

LAKE, B.M., YUEN, H.C., RUNGALDIER, H. & FERGUSON, W.E. 1977 Nonlinear deep-water waves: theory and experiment. Part 2. Evolution of a continuous wave train. *J. Fluid Mech.* **83** (1), 49–74.

LAX, P.D. 1973 *Hyperbolic Systems of Conservation Laws and the Mathematical Theory of Shock Waves*. SIAM.

LO, E. & MEI, C.C. 1985 A numerical study of water-wave modulation based on a higher-order nonlinear Schrödinger equation. *J. Fluid Mech.* **150**, 395–416.

MA, Y., DONG, G., PERLIN, M., MA, X. & WANG, G. 2012 Experimental investigation on the evolution of the modulation instability with dissipation. *J Fluid Mech.* **711**, 101–121.

MELVILLE, W.K. 1982 The instability and breaking of deep-water waves. *J. Fluid Mech.* **115**, 165–185.

OMURA, Y. 2021 Nonlinear wave growth theory of whistler-mode chorus and hiss emissions in the magnetosphere. *Earth, Planets Space* **73** (1), 1–28.

OMURA, Y., KATOH, Y. & SUMMERS, D. 2008 Theory and simulation of the generation of whistler-mode chorus. *J. Geophys. Res. Space Phys.* **113** (A4), A04223.

ONORATO, M., OSBORNE, A.R., SERIO, M., RESIO, D., PUSHKAREV, A., ZAKHAROV, V.E. & BRANDINI, C. 2002 Freely decaying weak turbulence for sea surface gravity waves. *Phys. Rev. Lett.* **89** (14), 144501.

RATLIFF, D.J. 2017 Conservation laws, modulation and the emergence of universal forms. PhD thesis, University of Surrey, UK.

RATLIFF, D.J. 2019 Dispersive dynamics in the characteristic moving frame. *Proc. R. Soc. Lond. A* **475** (2223), 20180784.

RATLIFF, D.J. 2021 Genuine nonlinearity and its connection to the modified Korteweg–de Vries equation in phase dynamics. *Nonlinearity* **35** (1), 30–65.

RATLIFF, D.J. & ALLANSON, O. 2023 The nonlinear evolution of whistler-mode chorus: modulation instability as the source of tones. *J. Plasma Phys.* **89** (6), 905890607.

RATLIFF, D.J. & BRIDGES, T.J. 2016*a* Multiphase wavetrains, singular wave interactions and the emergence of the Korteweg–de Vries equation. *Proc. R. Soc. Lond. A* **472** (2196), 20160456.

RATLIFF, D.J. & BRIDGES, T.J. 2016*b* Whitham modulation equations, coalescing characteristics, and dispersive Boussinesq dynamics. *Physica D Nonlinear Phenom.* **333**, 107–116.

SHUGAN, I., KUZNETSOV, S., SAPRYKINA, Y., HWUNG, H.H., YANG, R.Y. & CHEN, Y.-Y. 2019 The permanent downshifting at later stages of Benjamin–Feir instability of waves. *Pure Appl. Geophys.* **176** (1), 483–500.

SLUNYAEV, A.V. 2005 A high-order nonlinear envelope equation for gravity waves in finite-depth water. *J. Expl Theor. Phys.* **101** (5), 926–941.

SU, M.-Y., BERGIN, M., MARLER, P. & MYRICK, R. 1982 Experiments on nonlinear instabilities and evolution of steep gravity-wave trains. *J. Fluid Mech.* **124**, 45–72.

VENAKIDES, S. 1986 Long time asymptotics of the Korteweg-de Vries equation. *Trans. Am. Math. Soc.* **293** (1), 411–419.

WHITHAM, G.B. 1967 Non-linear dispersion of water waves. *J. Fluid Mech.* **27** (2), 399–412.

WHITHAM, G.B. 2011 *Linear and Nonlinear Waves*. John Wiley & Sons.

YUEN, H.C. & FERGUSON, W.E.Jr. 1978 Relationship between Benjamin–Feir instability and recurrence in the nonlinear Schrödinger equation. *Phys. Fluids* **21** (8), 1275–1278.

YUEN, H.C. & LAKE, B.M. 1982 Nonlinear dynamics of deep-water gravity waves. *Adv. Appl. Mech.* **22**, 67–229.